A K-band Spoof Surface Plasmon Polaritons Bandstop Filter with Capacitively Loaded Split-ring Resonator

Peng Chen [1,2], Luping Li [1], Zhijie Wang [1], and Kai Yang [1,2*]

[1] School of Aeronautics and Astronautics
University of Electronic Science and Technology of China, Chengdu, 611731, P. R. China

[2] Aircraft Swarm Intelligent Sensing and Cooperative Control
Key Laboratory of Sichuan Province, Chengdu, 611731, P. R. China
kyang@uestc.edu.cn

Abstract ─ A K-band bandstop filter based on the spoof surface plasmon polaritons (SPP) and the capacitively loaded split-ring resonator (RSS) is proposed in this paper. The capacitively loaded RSS consists of two parts: the traditional rectangle RSS and a T-type stub placed at the center of the arm microstrip line of the rectangle RSS. Thanks to the capacitively loaded RSS, the operating frequency of the resonator is reduced, which is helpful for miniaturizing the circuit size. The dispersion feature of the capacitively loaded RSS is studied by simulation and the geometrical parameters effects on the filter's final performance are discussed. A K-band bandstop filter with spoof SPP and capacitively loaded RSS is designed, fabricated and measured to verify the proposed design methodology. The measured results show that the bandstop filter works at 21.05 GHz-22.95 GHz with more than 40 dB insertion loss.

Index Terms ─ Bandstop filter, capacitively loaded stub, split-ring resonator, spoof surface plasmon polaritons.

I. INTRODUCTION

The classical surface plasmon polariton (SPP) is a kind of electromagnetic (EM) wave which transmits along the metal-air interface in the infrared and visible frequency [1]. Comparing with the traditional microstrip line, the classical SPP has less radiation loss since the EM wave vertical to the metal-air interface attenuates exponentially. It is considered as a promising structure for high-frequency EM wave transmission and widely applied on various optical components design [2-4]. However, the SPP only exists at far-infrared range. In order to make the SPP work at radio frequency (RF) and microwave frequency, various planer spoof SPPs, which have the similar characters of the natural SPP, have been invented in recent years [5].

The bandstop filter, also named as notch filter or reject filter, plays an important role in wireless communication system for its ability to suppress harmonic or unwanted wave, reduce mutual coupling and decrease spurious and leakage transmission [6]. The traditional planer bandstop filter design methods include bandstop stubs, defected ground structures, split-ring resonator, non-resonating nodes filters, extracted pole techniques and coupled resonator and so on. Traditional planer bandstop filters have serious dielectric loss at K-band and even higher-frequency band, resulting large heating in the dielectric material and EM radiation.

As mentioned above, the planer spoof SPP is a low dielectric loss structure and can be designed to pass or stop specified spectrum. The spoof bandstop filter is one of these applications. There are several reported works about the spoof SPP bandstop filter [7-15]. The first reported spoof SPP bandstop filter etched the additional resonator at the backside of the spoof SPP transmission line or at the top side of each stubs of the spoof SPP structure [7]. Soon this work was extended to the tunable metamaterials [8]. A spoof SPP bandstop filter was designed by adding the circular resonator with special holes at the side of the spoof SPP transmission line [9]. Another reported work placed the complementary SRR unit between two stubs of the spoof SPP transmission line for better rejection performance [10]. Furthermore, using the H-shape structures metamaterial particle, the double-side corrugated spoof SPP transmission line also showed bandstop features [11]. Ref [12] verified that by placing a conventional microstrip at the bottom center of a symmetrically periodically corrugated metallic strip showed the similar feature of the localized spoof surface plasmon and can be used to design bandstop filter. The single SRR unit set between two neighboring stubs of the spoof SRR transmission line also was can be applied for

Submitted On: July 25, 2019
Accepted On: February 12, 2020

bandstop filter [13]. Then a spoof SPP bandstop filter with the three different type folded split-ring resonator were presented to design dual-band and tri-band bandstop filter [14]. All these reported spoof SPP bandstop filters have similar performance and design methodologies, such as adding special unit between two neighboring stubs of the spoof SRR transmission line to get the bandstop unit, which is the fundamental base for the bandstop filter design, and controlling the bandstop filter's performance by just adjusting the parameters of their bandstop unit.

Inspired by these above-mentioned works, a novel spoof SPP bandstop filter is proposed in this paper. A capacitively loaded RSS is set between two neighboring stubs of the spoof SRR transmission line. Furthermore, the capacitively loaded RSS and the two neighboring stubs of the spoof SRR transmission line work together as a bandstop unit. The capacitively loaded RSS could reduce the resonating frequency of the bandstop unit and bringing in extra design freedom to optimize the filter's performance.

II. FILTER DESIGN

The traditional spoof SPP filter is displayed in Fig. 1. It consists of three parts. The first part is the standard 50 Ω microstrip line as the input/output port. The third part is the spoof SPP transmission line which is composed of the same height vertical stubs and a horizontal microstrip line connecting these vertical stubs together. The second part is the mode transfer part which transfer the quasi-TEM mode of the microstrip line to the spoof SPP mode of the spoof SPP transmission line.

The traditional spoof SPP unit has the lowpass feature and the cut-off frequency is decided by the height of the stubs. As the stubs become longer, the cut-off frequency becomes lower and vice versa. If an RSS unit is placed between the two neighboring stubs of the spoof SPP transmission line, the new structure performs bandstop feature. This phenomenon can be explained as follows. As the traditional strip-line bandstop filter, the SRR unit is capacitively coupled to the main EM transmission structure. The main EM transmission line is the spoof SPP transmission line in the spoof SPP bandstop filter while it is the microstrip line in the traditional strip-line bandstop filter. The capacitively coupling is realized by the physical circuit gap between the SRR and the main EM transmission line. The SRR performs as the serial LC circuit and often is realized by one quarter open stub.

Since the rejected frequency of the whole bandstop filter is determined by the resonating frequency of the SRR, the circuit miniaturization can be achieved by reducing the resonating frequency of the SRR. The T-type stub is inserted in the center of the horizontal arm of the SRR structure. It brings in three design freedom. The SRR, the T-type stubs and the two neighboring stubs of the spoof SRR transmission line work together to be as a bandstop filter's fundamental resonating unit, which is shown in Fig. 2. The whole bandstop filter is illustrated in Fig. 3.

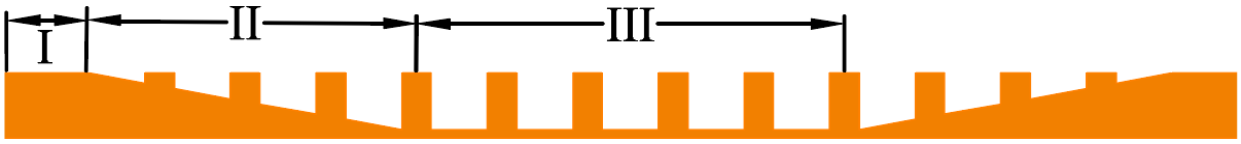

Fig. 1. The schematic of the traditional lowpass spoof SPP filter.

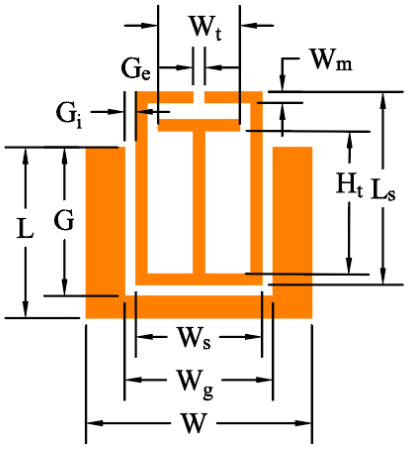

Fig. 2. Schematic of the proposed spoof SPP bandstop filter resonating unit.

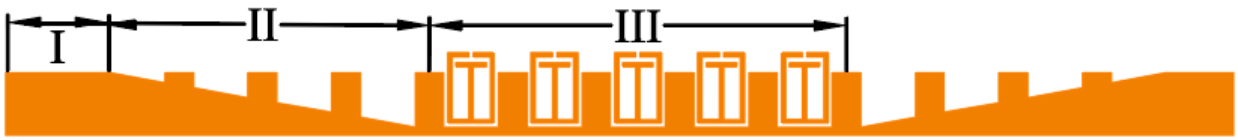

Fig. 3. The schematic of the proposed spoof SPP based bandstop filter with capacitively loaded RSS.

A. Dispersion analysis

To understand the performance of the whole bandstop filter, the dispersion of the single bandstop resonating unit shown in Fig. 2 is analyzed. The initial parameters of this unit are set as follows. The stub height G is 1.34 mm. The height L is 1.54 mm. The length of the comb-shaped unit W_g is 1.34 mm. The length W is 2.04 mm. The length W_s is 1.14 mm. The gap G_i and G_e are both 0.1 mm. The length W_t is 0.74 mm. The height H_t is 1.29 mm. All the line widths of the bandstop resonating unit are 0.1 mm. The dielectric coefficient of the substrate is 2.2 and the height of the substrate is set as 0.508 mm. Back of the substrate is covered by the annealed copper.

The Floquet method in the CST Microwave Studio® full-wave electromagnetic simulating platform is used to study the dispersion of the bandstop resonating unit. The simulated results are shown in Fig. 4. The fundamental, second harmonic and third harmonic modes of the proposed bandstop resonating unit are named as mode 1, mode 2 and mode 3 in Fig. 4, respectively. The black dot line is the dispersion of the calculated EM wave in the vacuum and the black dash line is the fundamental mode of the traditional spoof SPP unit for comparing purpose. There is gray frequency gap between the model 1 and mode 2, which is the bandstop spectrum of the proposed bandstop resonating unit. It is very safe to predict that the filter based on the proposed bandstop resonating unit has a rejection bandwidth between 22 GHz and 23 GHz. Furthermore, the cut-off frequency of the final filter based on the bandstop resonating unit is about 27 GHz since it is determined by the cut-off frequency of the traditional spoof SPP.

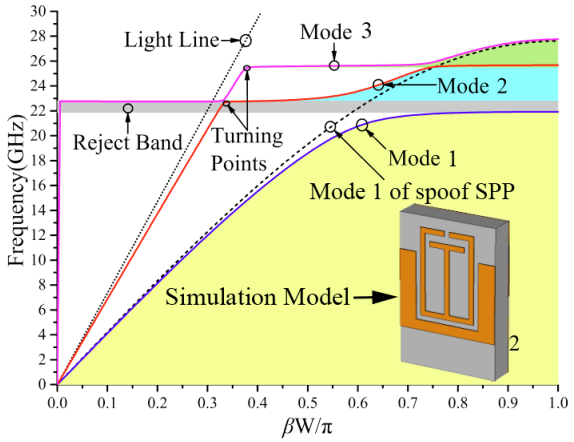

Fig. 4. Dispersion simulation of the spoof SPP unit.

It is note that the cut-off frequency of the proposed bandstop resonating unit is much lower than that of the EM wave in vacuum, which means that this unit behaves slow-wave feature, which is typical feature of the spoof SPP.

B. Equivalent circuit model

To theoretically understand the resonating frequency, the equivalent circuit model is built in Fig. 5, where ML is the microstrip line, CML is the coupling microstrip line, respectively. The ML1 and CML1 are utilized to simulate the performance of the coupling effect between the left-side stub and the left-side rectangle SRR while the ML2 and CML2 are utilized to simulate the feature of the coupling effect between the right-side stub and right-side rectangle SRR. The ML2, ML3 and ML4 are used to simulate the performance of the T-type stubs.

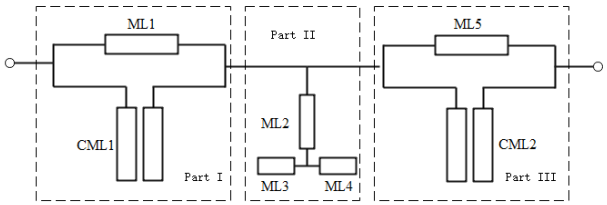

Fig. 5. Equivalent circuit model of the proposed spoof SPP filter unit.

The characteristic impedance of ML1, ML2, ML3 and ML4 is Z_{L1}, Z_{L2}, Z_{L3} and Z_{L4}, the corresponding electric length is θ_{L1}, θ_{L2}, θ_{L3} and θ_{L4}, the even-mode and odd-mode characteristic impedance of CML1 is z_{pe} and z_{po} and the corresponding electric length is θ_{pe} and θ_{po}, respectively. The structure of the whole circuit is centrosymmetric and the parameters of the ML1 and ML5, CML1 and CML2 are the same. Now the part I in Fig. 5 is discussed.

The ABCD matrix of ML1 is:

$$F_1 = \begin{bmatrix} \cos(\theta_{L1}) & jZ_{L1}\sin(\theta_{L1}) \\ j\sin(\theta_{L1})/Z_{L1} & \cos(\theta_{L1}) \end{bmatrix}. \quad (1)$$

The ABCD matrix of CML1 is:

$$F_2 = \begin{bmatrix} \dfrac{Z_{pe}\cot(\theta_{pe})+Z_{po}\cot(\theta_{po})}{Z_{pe}\cot(\theta_{pe})-Z_{po}\cot(\theta_{po})} & -j\dfrac{2Z_{pe}Z_{po}\cot(\theta_{pe})\cot(\theta_{po})}{Z_{pe}\cot(\theta_{pe})-Z_{po}\cot(\theta_{po})} \\ j\dfrac{2}{Z_{pe}\cot(\theta_{pe})-Z_{po}\cot(\theta_{po})} & \dfrac{Z_{pe}\cot(\theta_{pe})+Z_{po}\cot(\theta_{po})}{Z_{pe}\cot(\theta_{pe})-Z_{po}\cot(\theta_{po})} \end{bmatrix}. \quad (2)$$

The ABCD matrix of part II is:

$$F_3 = \begin{bmatrix} 1 & 0 \\ Y_{p2} & 1 \end{bmatrix}, \quad (3)$$

where Y_{p2} is the conductance of ML2, ML3 and ML4. Considering $Z_{L3} = Z_{L4}$ and $\theta_{L3} = \theta_{L4}$, we have:

$$Y_{p2} = \frac{j}{Z_{L2}} \frac{Z_{L2} + Z_{L3}\cot(\theta_{L3})\tan(\theta_{L2})}{Z_{L3}\cot(\theta_{L3}) - Z_{L2}\tan(\theta_{L2})}. \quad (4)$$

The ABCD matrix of the whole circuit is:

$$F = \begin{bmatrix} A & B \\ C & D \end{bmatrix} = F_1F_2F_3F_2F_1. \quad (5)$$

The resonating condition is:

$$Y = \frac{C}{A} = 0, \quad (6)$$

which can be changed as:

$$\begin{cases} \text{Real}(Y) = 0 \\ \text{Imag}(Y) = 0 \end{cases}. \quad (7)$$

For simplification, we set $\theta_{pe} = \theta_{po} = \theta_p$. The real part of Y is identical with 0. We just need to make sure the imaginary part of Y is equal to zero. As a matter of fact, the numerator of the imaginary part of Y can be written as:

$$\begin{aligned} &\tan(\theta_{L3})*((Z_{pe} + Z_{po})Z_{L1}\cos(\theta_{L1}) \\ &+ 2Z_{pe}Z_{po}\cot(\theta_p)\sin(\theta_{L1})Y_{i3} = 0 \end{aligned}, \quad (8)$$

where Y_{i3} is a very complicated function of the above-mentioned parameters and it is impractical to control this complicated express to reach the resonating condition.

i) If θ_{L3} is not equal to 0, the resonating condition is decided as follow:

$$\frac{\tan(\pi - \theta_{L1})}{\tan(\theta_p)} = \frac{(Z_{pe} + Z_{po})Z_{L1}}{2Z_{pe}Z_{po}}, \quad (9)$$

which means that the resonating condition of the proposed bandstop resonating unit is only related with the rectangle SRR and the stubs of the spoof SPP.

ii) If θ_{L3} is equal to 0, the bandstop resonating unit also can resonate.

It is worthy to note that the proposed equivalent circuit model is only roughly simulate the real circuit. It does not mean that the T-type stub is not related with the performance of the proposed filter. It provides import information that the stop bandwidth is mainly predicted by the coupling between the stub from the spoof SPP and the rectangle SRR. We can design the parameters of the stubs of the traditional spoof SPP transmission line and the rectangle SRR and then add the T-type stub for optimizing the final performance.

B. Filter design

As the traditional spoof SPP lowpass filter in Fig. 1, the proposed spoof SPP bandstop filter is also composed of three parts: Part I, Part II and Part III, which is shown in Fig. 3. Part I is a 50 Ohm microstrip line as the input/output port, which transmits the quasi-TEM wave. Part III is the spoof SPP transmission line part which contains five periodically arranged proposed units and transmits spoof SPPs wave. This part is the key of the filter which determines the final feature of the proposed bandstop filter. Part II is a mode conversion part which transforms the quasi-TEM of the microstrip line to the spoof SPPs wave of the spoof SPP part. The whole structure of the proposed filter is centrosymmetric.

The filter is designed on Rogers 5880 substrate with 2.2 dielectric coefficient and 0.508 mm height. It is simulated in CST Microwave Studio® and the simulation results are illustrated in Fig. 5. According to simulated S_{21}, a rejection band is inserted in the low-pass band. Accordingly, the proposed filter has the bandstop feature as previous dispersion analysis. In the bandstop band, 3 dB rejection points are 21.32 GHz and 22.94 GHz, respectively. The center frequency of the bandstop band is 22.13 GHz and 3 dB bandstop bandwidth is 1.62 GHz. The maximal rejection depth is 46.5 dB.

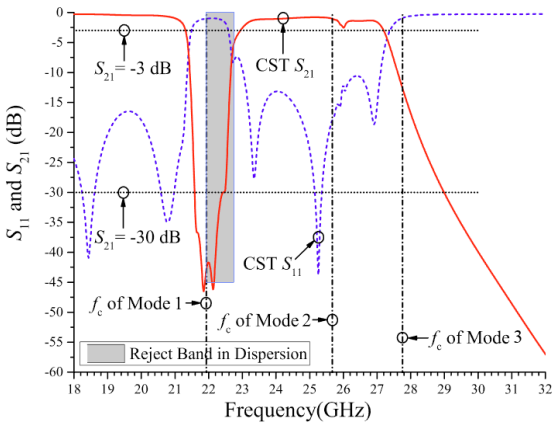

Fig. 5. Simulated S_{11} and S_{21} of the proposed filter. The gray band is bandstop band in dispersion of the proposed unit and f_c is cut-off frequency.

In the first passband, when the frequency increases from 10 GHz to 20.5 GHz, the insertion loss changes from 0.16 dB to 0.52 dB. In the second passband, the maximal insertion loss is 2.5 dB at the depression point and the minimal insertion loss is 0.9 dB. Moreover, 3 dB cut-off frequency of the filter is 27.2 GHz and the out-of-band rejection can reach more than 60 dB.

The gray region in Fig. 5 is the rejection band predicted by the dispersion analysis, which is in the rejection band of the final filter. In addition, the high cut-off frequency of the simulated rejection band is close to the predicted high cut-off frequency of the dispersion analysis while the low cut-off frequency of the simulated rejection band is lower than that of the dispersion results, which may be caused by the added T-type stub. In mode 1 and mode 3, both the cut-off frequencies are in the rejection band, which proves correspondence between

rejection bands of the modes and the filter. In mode 2, depression point in S_{21} is near the cut-off frequency of the mode, which proves that the cut-off effect of mode 2 functions and it degrades S_{21} of the filter. In summary, the bandstop band and the cut-off points of dispersion agree with the filter, which proves effectiveness of the proposed spoof SPPs unit and filter design approach.

C. Performance of capacitively loaded RSS

One of the main differences of the proposed spoof SPP bandstop filter is to add a T-type stub into the rectangle RSS to increase the spurious suppression and reduce the resonating frequency. As illustrated in Fig. 6, the spoof SPP filter with capacitively loaded RSS with T-type stub has lower resonating frequency than the spoof SPP filter with single SRR. Moreover, the spurious of the spoof SPP filter with capacitively loaded SRR with T-type stub has 5 dB lower than the spoof SPP filter with single RSS in the left side of the rejection band while the spurious suppressions of the right sideband keep the same.

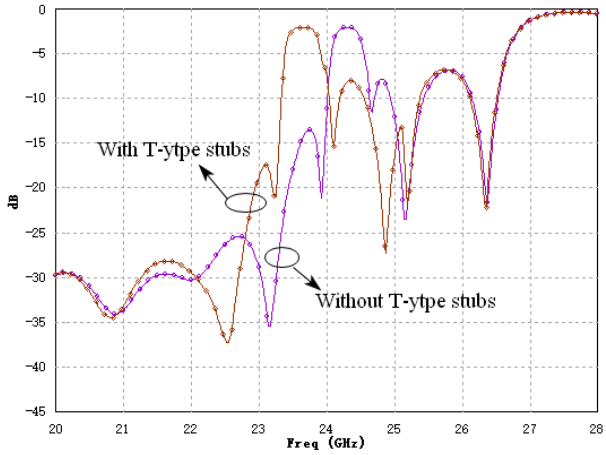

Fig. 6. The simulated results of the spoof SPP bandstop filter with/without the T-type stubs.

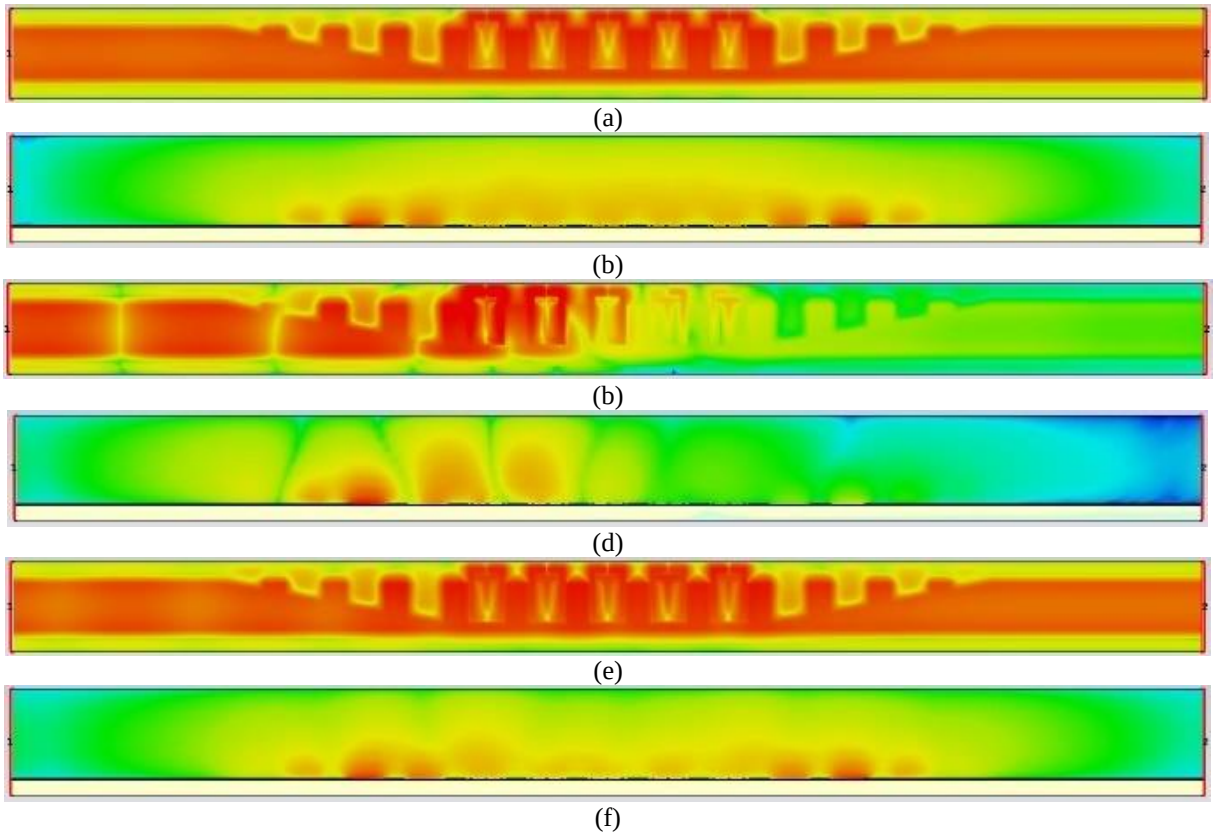

Fig. 7. The simulated electric fields of the spoof SPP filter: (a) top view of the passband at 19 GHz, (b) side view of the passband at 19 GHz, (c) top view of the stopband at 21 GHz, (d) side view of the stopband at 21 GHz, (e) top view of the passband at 24 GHz, and (f) side view of the passband at 24 GHz.

Figure 7 displays the simulated electric field of the spoof SPP filter with capacitively loaded SRR. It can be seen from the two side view figures at 19 GHz, 21 GHz and 24 GHz that most the energy is restricted near the surface of the substrate, which is similar of the natural SPP material. The energy passes through the proposed

spoof SPP filter with capacitively loaded SRR at the passband frequency while the energy reflects to the input port at the stopband frequency. It is proved that the proposed filter performs bandstop feature.

III. FILTER MEASUREMENT

To verify the proposed design method, a bandstop filter based on the proposed spoof SPP transmission line with capacitively loaded SRR is designed and fabricated on Rogers RT/duroid® 5880 with dielectric coefficient of 2.2 and height of 0.508 mm. The photograph of the fabricated filter is displayed in Fig. 8. The whole size of the filter is 40 mm×3 mm. The filter is embedded in a 3.0 mm high aluminum box and connects with 2.92 mm connectors.

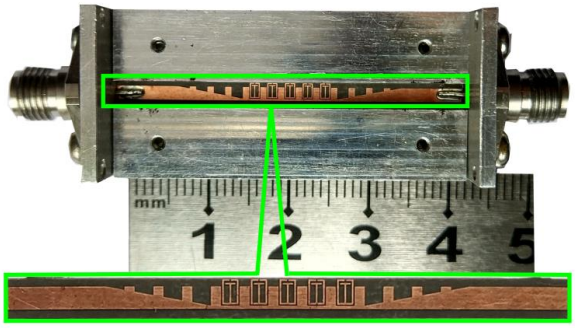

Fig. 8. Photograph of the fabricated filter embedded in an aluminum box.

Measurement results are obtained by the Ceyear® AV3672C vector network analyzer and illustrated in Fig. 9. The simulation results agree with the measurement results except the insertion loss and a little frequency shift to the left side of the designed stopband. As shown by the measured results, the stopband is from 21.05 GHz to 22.95 GHz and the stopband bandwidth is 1.90 GHz. The maximal return loss is 41.8 GHz at 21.8 GHz.

The high insertion loss of the fabricated filter is mainly caused by the substrate dielectric loss. Although the dielectric loss of the spoof SPP transmission line is lower than the microstrip line. However, the length of the fabricated bandstop filter is quite long for adjustment and assembly. In order to proof this point, a microstrip line with the same length of the fabricated bandstop filter and 50 Ohm characteristic impedance is fabricated and measured. The results are illustrated in in Fig. 10. The average insertion losses of simulation and measurement are 0.33 and 1.78 dB, respectively, which has 1.45 dB difference. Also, the worst insertion loss is about 2.5 dB at 21 GHz, which is near the designed stopband. For comparison, the measured S_{21} subtracting the loss of the microstrip line with 50 Ohm impedance is shown in Fig. 11. It is clear that the transmission loss of the spoof SPP near the stopband is very low as predicted.

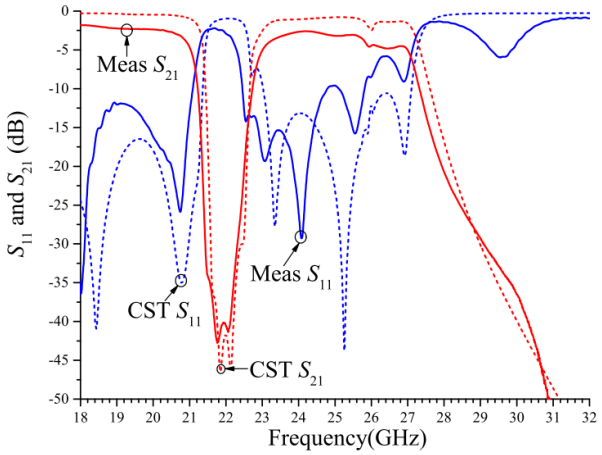

Fig. 9. Measured and simulated S_{11} and S_{21} results of the fabricated filter.

The left and right cutoff frequency of the measured stopband are lower than the measured ones, respectively. The frequency shift is about 0.9% of the central frequency, which is at normal frequency. The difference is mainly caused by the nonideal effect of the substrate and the fabrication tolerance.

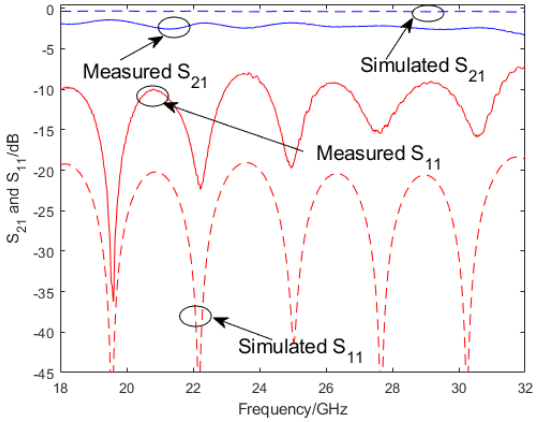

Fig. 10. Measured and Simulated S_{11} and S_{21} of the 50 Ohm microstrip line with the same length of the fabricated filter.

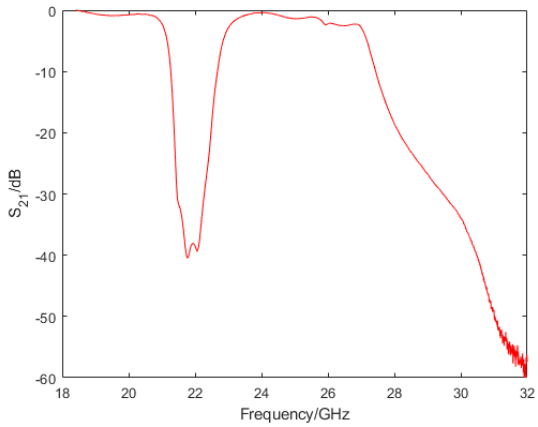

Fig. 11. The measured S_{21} subtracting the loss of the microstrip line with 50 Ohm impedance.

IV. CONCLUSION

This paper presents a novel spoof SPP bandstop filter with capacitively loaded SRR. The dispersion mode is the discussed and the capacitively loaded SRR's effect to the filter feature is studied. In both simulation and measurement, the filter shows a steep and wide rejection band in an ultra-wide low-pass band, which agree with dispersion of the proposed bandstop resonating unit. The fabricated filter has a 1.9 GHz rejection band and 41.8 dB insertion loss at the designed bandwidth. The center frequency of the rejection band is 22.0 GHz.

ACKNOWLEDGMENT

This work was supported by the National Natural Science Foundation of China 61601088 and 61571093 and the Fundamental Research Funds for the Central Universities ZYGX2019J085.

REFERENCES

[1] A. Bostwick, F. Speck, T. Seyller, et al., "Observation of plasmarons in quasi-freestanding doped graphene," *Science*, vol. 328, no. 5981, pp. 999-1002, May 2010.

[2] J. O'Hara, R. Averitt, and A. Taylor, "Terahertz surface plasmon polariton coupling on metallic gratings," *Opt. Lett.*, vol. 12, no. 25, pp. 6397-402, Dec. 2004.

[3] J. B. Pendry, L. M. Moreno, and F. J. Garcia-Vidal, "Mimicking surface plasmons with structured surfaces," *Science*, vol. 305, no. 5685, pp. 847-848, Aug. 2004.

[4] J. T. Shen, P. B. Catrysse, and S. Fan, "Mechanism for designing metallic metamaterials with a high index of refraction," *Phys. Rev. Lett.*, vol. 94, no. 19, p. 197401, May 2005.

[5] X. P. Shen and T. J. Cui, "Planar plasmonic metamaterial on a thin film with nearly zero thickness," *Appl. Phys. Lett.*, vol. 102, no. 21, p. 83, May 2013.

[6] A. D. Vala, A. V. Patel, A. Patel, "Design and analysis of microstrip bandstop filter based on defected ground structure," *Int. J. of Eng. Res. Tech.*, vol. 3, no. 5, pp. 63-66, May 2013.

[7] B. C. Pan, Z. Liao, J. Zhao, et al., "Controlling rejections of spoof surface plasmon polaritons using metamaterial particles," *Opt. Lett.*, vol. 22, no. 11, pp. 13940-50, 2014.

[8] J. Xu, H. C. Zhang, W. X. Tang, et al., "Transmission-spectrum-controllable spoof surface plasmon polaritons using tunable metamaterial particles," *Phys. Rev. Lett.*, vol. 108, no. 19, pp. 824-848, May 2016.

[9] B. G. Xiao, S. Kong, and S. H. Xiao, "Spoof surface plasmon polaritons based notch filter for ultra-wideband microwave waveguide," *Opt. Comm.*, vol. 374, pp. 13-17, Sep. 2016.

[10] Q. Zhang, C. H. Zhang, Y. Y. Jia, et al., "A series of compact rejection filters based on the interaction between spoof SPPs and CSRRs," *Sci. Rep.*, vol. 6, p. 28256, June 2016.

[11] Q. Zhang and T. J. Cui, "Rejection filters based on spoof surface plasmons and complementary meta-material particles," In *IEEE MTT-S Int. Microw. Workshop Series on Adv. Materials and Processes for RF and THz App.*, pp. 1-3, 2016.

[12] B. Z. Xu, Z. Li, L. L. Liu, et al., "Bandwidth tunable microstrip band-stop filters based on localized spoof surface plasmons," *J. Opt. Soc. Am. B*, vol. 33, no. 7, pp. 1388-1391, July 2016.

[13] S. M. Zhao, H. C. Zhang, J. H. Zhao, et al., "An ultra-compact rejection filter based on spoof surface plasmon polaritons," *Sci. Rep.*, vol. 7, no. 1, p. 10576, July 2017.

[14] L. Li, L. Dong, P. Chen, et al., "Multi-band rejection filters based on spoof surface plasmon polaritons and folded split-ring resonators," *Int. J. Microw. Wirel. Tech.*, vol. 11, no. 8, pp. 774-781, Aug. 2019.

Peng Chen received the bachelor's degree and the Ph.D. degree from University of Electronic Science and Technology of China (UESTC), Chengdu, China, in 2009 and 2015, respectively. He then became a Lecturer and an Associate Professor in the School of Aeronautics and Astronautics, UESTC, in 2015 and 2019, respectively. During Nov. 2017 to Nov. 2018, he was a Visiting Researcher in Tohoku University, Sendai, Japan. He is

a member of Chinese Institution of Electronics and a member of IEEE.

His research interests include microwave and wireless communication components design and weak electromagnetic fields detection.

Luping Li received his bachelor's degree from Chengdu University of Information Technology, Chengdu, China in 2016 and master's degree from the University of Electronic Science and Technology of China (UESTC), Chengdu, China in 2019. Now he is studying his Ph.D. degree in UESTC.

His research interests are RF/microwave filters.

Kai Yang received his bachelor's degree and master's degree from University of Electronic Science and Technology of China, Chengdu, P. R. China, in 1993 and 2000, respecttively, where he then became the Associate Professor and the Full Professor in 2001 and 2007, respectively. He is a senior member of Chinese Institution of Electronics.

His research interests are RF/microwave circuits and systems, superconducting microwave application.